25. We thank T. and M. Kohler and Windway Foundation, Inc., for time, organizational expertise, funds, and resources that ranged from computers to helicopters. Contributions of time and funds by more than 150 volunteers made this project possible. We thank the various paleontological and geological staffs for assistance. We are grateful to landowners near Glendive, MT, and Marmarth, ND, for permitting work on their properties. Access to public lands was granted by the U.S. Bureau of Land Management and the Montana Department of State Lands. Special thanks are due to M. Davis and M. Sullivan for greatly facilitating our work in Makoshika State Park. Partial funding, support, and supplies were provided by Friends of the Milwaukee Public Museum, the Department of Geology, University of Rhode Island, Marquette Electronics Foundation, Beatrice Foods, Johnsonville Sausages, Coleman Outdoor Products, and Igloo Corporation. We thank W. P. Coombs, J. H. Ostrom, R. E. Johnson, C. G. Harding, O. S. Hill, J. R. Miller, D. J. Stephenson, and K. Wendt for their assistance with this project. While not necessarily sharing our conclusions, J. D. Archibald, J. A. Cain, S. L. D'Hondt, T. Webb III, and two anonymous reviewers read drafts of this manuscript.

22 April 1991; accepted 13 August 1991

Structural Control of Flank Volcanism in Continental Rifts

MICHAEL ELLIS AND GEOFFREY KING

Many volcanoes emerge from the flank (footwall) of normal faults in continental rift zones. Because such locations are commonly topographically high and exhibit minor compressional structures, the association is enigmatic. A simple flexing plate model shows that deformation of a flexurally supported upper crust during normal faulting generates a dilational strain field in the footwall at the base of the crust. This strain field allows cracking and tapping of preexisting melt.

A COMMON OBSERVATION IN REGIONS of continental extension is the occurrence of flank volcanism, in which volcanism and associated shallow level intrusions are found in the footwalls of normal faults. The association is temporal as well as spatial. Volcanism is generally active as long as the fault is active, and, as fault activity migrates, so too does volcanism. These observations suggest that there is a coupling between processes of brittle deformation in the upper crust and those involving magma injection in the lower crust.

We explain this association with the use of a numerical model (*1*) in which the upper crust is modeled as an elastic beam with a reduced effective elastic thickness, and the lower crust behaves as a fluid. Deformation is driven entirely by gravity and includes the modifying effects of erosion and sedimentation.

The temporal and spatial association between normal faulting and volcanism is most evident in regions where crustal extension is active and in its early stages. For example, in the Taupo rift of North Island, New Zealand, two volcanoes, Mount Tarawera and Mount Edgecumbe, are on the footwall side of the major Edgecumbe-Onepu fault and outside the zone of active rifting (Fig. 1A). The fault last moved in the 1987 Edgecumbe magnitude $M_s \approx 6.3$ earthquake, and it offsets basement by ~1 km (*2*). In the 1987 fault scarp, Holocene soils are interlayered with volcanic ash derived from Mount Tarawera. Moreover, the Taupo eruptive event of ~A.D. 150, considered to be the largest volcanic eruption of the last 7000 years (*3*), appears to have occurred immediately to the southeast (in the footwall) of the main rift-bounding faults.

In the Rungwe volcanic field (Fig. 1B), part of the western arm of the East African rift system (*4*), the oldest source of volcanism associated with the rifting is late Miocene [~7 million years old (Ma)] and is sited on the flank of the rift-bounding Livingstone faults (*4*). Active rifting has migrated toward the axial zone, where a series of Pliocene and Quaternary volcanoes sit in the footwall of the active Mbaka fault system, the most prominent fault system in the axial zone. Extensive volcanism also occurred on the flanks of the Gregory rift [for example, the Kapiti volcanic rocks along the tilted Aberdare Range and basalts along the Nguruman escarpment (*5*)]. Farther north, in the Ethiopian rift, the Gorfu, Entotto, and Gara Mariam centers are further examples of flank volcanism (*6*). In general, volcanic activity throughout the eastern rift follows that of faulting (*5, 6*).

Another example comes from the active Long Valley magmatic complex (Fig. 1C). Present seismic activity under Mammoth Mountain (Figs. 1C and 2D) is confined to a well-defined dike-like shape below about 6 km; above this level, events spread laterally (*7*). Seismic swarms are typical in this region and are generally attributed to the development of a dike (*8*). Mammoth Mountain lies in the footwall of the active Sierra Nevada range-bounding normal fault (*9*), although this relation is partly obscured by the 700,000-year-old caldera rim.

In 1980, a series of moderate earthquakes occurred in the footwall of the active Hilton Creek fault (Figs. 1C and 3) that were characterized by significant non–double-couple focal mechanisms (*10*). Julian (*11*) suggested that these earthquakes were associated with active magmatic intrusion. During the early part of 1990, the resurgent dome within the caldera was extending at a rate five times that of normal (*12*), presumably from the motion and intrusion of magmatic material at depth. Both the resurgent dome and the initial vent for the Plinian deposit of the 700,000-year-old Bishop tuff are in the footwall of the Hilton Creek fault (*13*) (Fig. 1C). We suggest that the volcanic processes and associated seismicity within the Long Valley caldera complex are connected to the evolution of the main Sierra Nevada (Hilton Creek) range–front fault system.

There are many other examples from virtually every rift system in the world. These systems include the Latir volcanic field and the Spanish Peaks complex, which represent the early stage of extension in the Rio Grande rift, United States (*14*); early volcanism along the flanks of the Baikal rift, Soviet Union (*15*); early volcanism along the eastern margin of the Red Sea (*16*); basaltic magmatism along the eastern edge of the Basin and Range province, particularly the St. George field in southwest Utah, which lies in the footwall of the active Hurricane normal fault (*17*); middle Miocene and Pliocene volcanism in the Death Valley region, California (*1, 18*); Mount Etna, Sicily, which has an unusual location on the nonvolcanic side of an island arc (*19*) that may be explained by its position in the footwall of the active Messina normal fault; the Quaternary volcanic Chaine des Puys, which is related to Quaternary normal faulting near Clermont Ferrand that has reactivated structures associated with the Oligocene Limagne graben (*20*); and the large volcanic complexes of Mount Kilimanjaro, Mount Kenya, and Mount Elgon along the Gregory rift, East Africa (*5*).

The approach to modeling these structures follows from that used by King and Ellis (*1*). In the model the x_1 axis is vertical and positive downwards, and the x_3 axis is horizontal. Two horizontal gravitating interfaces are defined. One represents the earth's surface, and the second represents the base of the brittle layer. At $x_3 = -60$ km, the horizontal displacement along a vertical

M. Ellis, Center for Earthquake Research and Information, Memphis, TN 38152.
G. King, Institut de Physique du Globe de Strasbourg, Strasbourg, France.

boundary is fixed ($u_3 = 0$), and the shear stress is set to zero ($\sigma_{13} = 0$). At $x_3 = 48$ km, both shear and normal stresses are set to zero ($\sigma_{33} = \sigma_{13} = 0$) at a second vertical boundary. These conditions produce a stress-free floating block tethered at −60 km. The length of the block is sufficient in that details of the way in which boundary conditions are imposed do not affect the deformation in the region where faulting is introduced.

Displacement across the normal fault is driven by application of a shear stress, the magnitude of which is derived from the assumed initial state of stress within the crust. The model boundary conditions appear to be reversed from those in the real world, in which the fault is ultimately weak (and can sustain no shear stress over the long term) and the far-field value of σ_{33} is likely to lie between 0.5 and 1.0 times the value of σ_{11}. These boundary conditions, however, allow us to ignore the static aspect of the problem and examine only the changes caused by fault motion (*1*). Appropriate parameter values were chosen to model an extensional region such as the Basin and Range province (*21*) and are consistent with estimates of low flexural rigidity ($\sim 10^{20}$ N m) determined through independent methods [(*1*) and references therein].

We are using elastic models to explain processes that exceed the elastic limit that, in the real world, involve irreversible nonlinear effects. Such modeling can be appropriate under certain circumstances (*22*). In our model, each increment of fault motion can be thought of as being associated with an earthquake and can thus be appropriately modeled elastically. Between earthquakes, stress relaxes both at depth and partially within the brittle layer such that a long-term model is a plate of apparently reduced modulus overlying a fluid half-space. Many such events can be summed in a linear fashion, provided the overall geometry does not change, to produce a result that is the same as the one we calculate here by deforming a linear system in a single step.

The results show (Figs. 2 and 3) that the variation of areal strain ($\epsilon_{11} + \epsilon_{33}$) in the elastic layer as a consequence of a small fault displacement is such that dilation occurs at the base of the footwall and to the footwall side of the surface trace of the normal fault. This is true regardless of the location of density contrasts in the elastic plate (Fig. 2B). The effect of increasing flexural rigidity is to move the zone of maximum dilation farther away from the fault. Thus, an effective elastic thickness of 15 km (10^{22} N m) produces a maximum dilation ~25 km away from the surface trace of the fault. The footwall dilation due to normal faulting leads to a volume increase (provided that no strain occurs out of the plane of cross section) and the probable development of cracks and veins. We suggest that the location of volcanism is related to the existence of dilation and uplift at depth.

Melt can move into voids in the solid material if that melt already exists. In addition, however, two conditions associated with fault motion favor the formation of melt under the footwall as a result of locally decreasing pressure. First, as displacement occurs, the base of the brittle-elastic zone in the footwall rises, and material moves into the space created. The pressure is reduced ΔP_b in proportion to the lifting of the footwall Δh ($\Delta P_b = \Delta h \rho g$, where ρ is the density and g is acceleration due to gravity). Second, as buoyant melt ascends into fissures in the brittle-elastic layer, the pressure at the base of the brittle-elastic layer is reduced further, because the density of the partial melt in the fissures will be less than that in a similar column of the surrounding solid material. The difference in pressure between the base of fluid and solid columns of height h is $\Delta P_h = h \Delta\rho g$, where $\Delta\rho$ is the contrast in density between solid and melt. If the pressure at the ascending crack tip equals the surrounding rock pressure, and if the flow-induced viscous pressure drop is negligible, this pressure difference may appear at the base of the brittle-elastic layer, where it can enhance localized melting. If, alternatively, the pressure at the base of the brittle-elastic layer does not drop and is the same for solid and liquid, the fluid pressure at the crack tip must exceed the stress in the surrounding rock by the same ΔP_h; thus, crack extension is enhanced by hydrofracturing.

The propagation of a magma-driven dike has been analyzed in detail (*23*). Our model adds to these analyses, because it provides a site for the preferential initiation and development of dikes and explicitly incorporates the effect of the spatially varying strain field, which is neglected in analytical treatments (*23*). Thus, using the same parameters as those for the model in Fig. 2A, we modeled the strain field of an incipient dike, introduced as a stress-free vertical cut at the base of the footwall (Fig. 3). The stress-free cut is equivalent to the condition in which the local hydrostatic pressure gradient is the same in the melt and the solid rock and in which flow-induced viscous pressure drop can be ignored. In the early stages of dike formation (Fig. 3A), the crack tip produces a local region of dilation, which will enhance the formation of further cracks and allow melt to intrude shallower levels of the crust. Thus, the process continues, and the crack

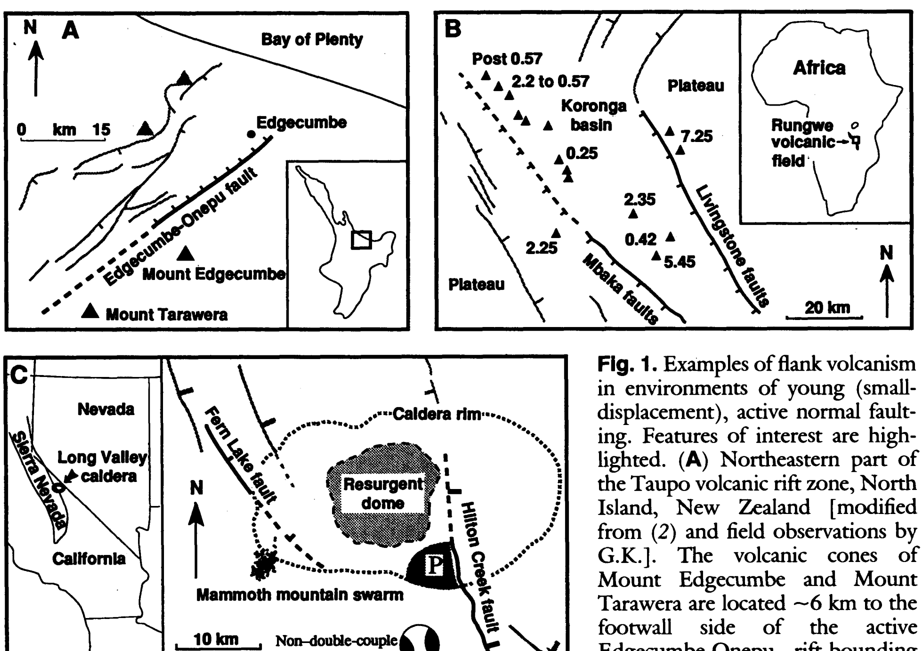

Fig. 1. Examples of flank volcanism in environments of young (small-displacement), active normal faulting. Features of interest are highlighted. (**A**) Northeastern part of the Taupo volcanic rift zone, North Island, New Zealand [modified from (*2*) and field observations by G.K.]. The volcanic cones of Mount Edgecumbe and Mount Tarawera are located ~6 km to the footwall side of the active Edgecumbe-Onepu rift-bounding fault. Elsewhere in the rift zone, volcanic activity is occurring to the footwall side of the active normal fault, and older inactive volcanoes lie in the footwall of rift-bounding normal faults. (**B**) Rungwe volcanic field in the western arm of the East Africa rift system [modified from (*4*)]. The oldest volcanic centers, ~7 Ma, are in the footwall of the main rift-bounding Livingstone faults. Younger volcanic centers (~5 to 0.25 Ma), with one exception, are similarly in the footwall of the younger Mbaka normal fault system. (**C**) Examples of probable active magmatic intrusions in the footwalls of major Sierra Nevada range-bounding normal faults in the Long Valley caldera region [modified from (*9*)]. The 1989–1990 Mammoth Mountain earthquake swarm is in the footwall of the Fern Lake fault; the non–double-couple earthquakes consistent with magmatic injection (*10, 11*), the vent (P) for the Plinian eruption of the 700,000-year-old Bishop tuff, and the active resurgent dome are all located in the footwall of the Hilton Creek fault.

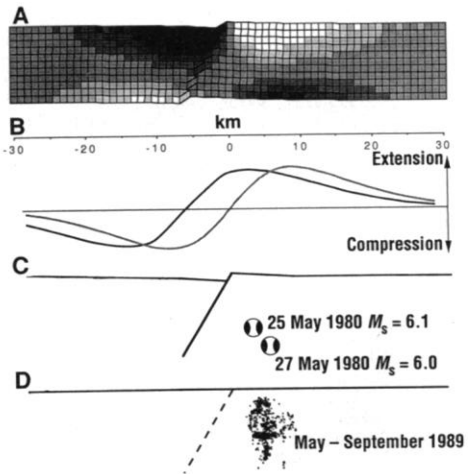

Fig. 2. (**A**) Distribution of strain and observations within the footwalls of relatively young (small-displacement) normal faults. Shaded with dilational strain at a 0.01 contour interval. Each grid unit is a square kilometer. Dark areas represent extension (areal increase); light areas contraction (areal decrease). Thus, if ϵ_{22} is zero, positive areal strains (ϵ_{11} + ϵ_{33}) lead to dilation. The strains are shaded from 0.5 km to a depth of 11.5 km and represent those due only to the motion across the fault and not to any preexisting condition or body forces. (**B**) Variation of dilational strain at a depth of 11 km is shown for the two limiting cases in which we assume either complete erosion and sedimentation (corresponding to no effective density contrast at the surface; light line) or no density contrast at depth (heavy line). Maximum extension at this depth occurs within the footwall and consistently to the footwall side of the surface trace of the fault. (**C**) Two moderate earthquakes in 1980 in the footwall of Hilton Creek fault (Fig. 1C) have been modeled as non–double-couple (*10*), which Julian (*11*) has interpreted as an indication of magmatic intrusion at depth M_s = surface wave magnitude. (**D**) An earthquake swarm under Mammoth Mountain between May and September 1989 shows a planar, dike-like distribution of small events below ~6 km and a more diffuse distribution at higher levels. When viewed in three dimensions and in chronological sequence, the events can be seen to begin at depths of ~9 km and migrate toward the surface up to ~2 km through May and June 1989. During these 2 months the events clearly define a northwest-striking planar form (Fig. 1C). Over the following 3 months, events above ~6 km were more distributed, and the planar form was confined to depths >6 km (*7*). This sequence of events is interpreted to represent the intrusion of a dike (*7, 8*).

(dike) propagates upward, resulting in a similar dilational strain field at the crack tip (Fig. 3, B and C). The strain field ahead of the crack tip overcomes the compressional strains that occupy the upper part of the elastic plate (compare Figs. 3A and 2, and Fig. 3, B and A). The compressional strains predicted by the model are seen in the field as minor reverse faults, folds, and shortening fabrics in the footwalls of normal faults (*1, 24*). Thus, dikes developed in the footwall of normal faults may transport melt through regions of local compression.

Models in which the crack tip was brought progressively closer to the surface all show the same dilation. These results indicate that the advancing fissure is able to reach the surface, provided that the depth-averaged hydrostatic pressure gradient is greater than the total viscous pressure drop. This process, combined with hydrofracturing, can explain why dikes rise through the footwall rather than elsewhere, even though they must pass through a compressional zone.

These mechanisms can tap such a melt or slightly alter preexisting conditions to create some melt. They cannot generate large quantities of melt. In many cases, the characteristics of footwall igneous rocks are consistent with a source magma that has spent time fractionating in the lower or middle crust [for example, (*3–6, 14–16, 18–20*)]. The isotopic characteristic of other flank volcanic rocks (particularly those erupted relatively late in the volcanic history) suggests quite primitive magmatic sources and a minimal residence time in the lower crust (*14, 17*). Such magmas likely have their source in the asthenosphere. We suggest that conduits through the upper crust are developed by the process described here, such that later, more primitive magmas simply follow the path of least resistance on the way to the surface. This conclusion is consistent, for example, with footwall volcanism in the Death Valley extensional region, where early magmas are relatively silicic and well fractionated, but later extrusives that erupted in the same footwall are relatively primitive (*25*).

If a source of melt is not available in the lower crust, we should not expect volcanism and shallow intrusion to be associated with normal faulting. This is consistent with patterns of volcanism in the Baikal, East African, and Rio Grande rifts, where volcanism is absent over large regions of extension. In other words, crustal extension by itself does not guarantee significant magma emplacement.

Some of the larger flank volcanoes along the Gregory rift are up to a hundred kilometers away from the active rift boundary, farther than our model predicts. Bosworth (*26*) has suggested that the origin of the large volcanic centers is related to the intersection of extension-related detachments (shear zones) with the asthenosphere. There is no evidence, however, that such deeply penetrating, discrete shear zones underlie regions of continental extension. This type of asymmetric shear zone model has been shown to be inappropriate for other better documented regions of extension (*27*). We prefer the explanation that the origin of the large volcanic centers is related to extension of the upper crust in the manner described here. The earlier rift boundaries may have been significantly wider than present-day boundaries, which is consistent with observations of narrowing rifts from, for example, the Red Sea (*15*) and Ethiopia (*6*). Alternatively, the prerifted crust in Africa may have had a significantly larger flexural rigidity than that of today, such that the maximum dilation at the base of the upper crust may have been tens of kilometers away from the surface trace of the normal faults. Indeed, the present-day African crust in the vicinity of the rift has a relatively high effective elastic thickness of ~21 to 36 km (*28*).

Volcanism is also influenced by other processes and structures. In the model described here, magma emplacement is structurally controlled by lift and the generation of dilational strains at the base of the upper crust during normal faulting. In the same sense, volcanism should be controlled by the development of dilational strains at depth caused by any upper crustal feature. Thus, irregular strike-slip faults (in zones of dilational steps or pull-aparts) will work in a similar way in the control of volcanism. For example, the location of the Inyo-Mono volcanic centers, California, is a result of a pull-apart fault pattern along the partly

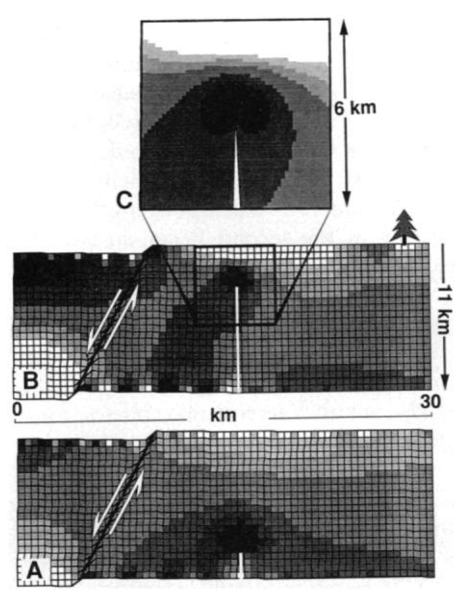

Fig. 3. Deformation of elastic plate due to relatively small displacement on a high-angle normal fault and in response to a tensional crack of designated lengths at the base of the footwall. Shading parameters as in Fig. 2. In (**A**) the crack, which has zero normal and tangential stress specified on its surfaces, rises 3 km from the base of the elastic layer, and in (**B**) it rises to 3 km from the surface. A detail of the strain field adjacent to the crack tip is shown in (**C**). The crack is able to dilate previously compressed material, thereby allowing the transport of magma through the locally shortened footwall.

strike-slip Sierran frontal fault system (*29*).

In the model, we also implicitly assume that the thermal structure of the crustal section is homogeneous. Heterogeneities in the thermal structure will be produced by continued extension of the upper crust, such that the geothermal gradient will eventually be higher immediately below the rift basin. For this reason, flank volcanism appears to be related most clearly to the early phases of extension, and later volcanism erupts through the axial zones of rifts (*4–6*).

Despite the foregoing qualifications, flank volcanism has been noted by field geologists in many environments and has seemed to defy simple explanation. The explanation we offer is simple and consistent with a model that explains other mechanical features of normal faulting (*1*). We assume that melt with some mantle affinities exists in parts of the lower crust. Such a hypothesis is consistent with recent observations that minor hot spots resulting from mantle processes are much more numerous on the Pacific floor than previously believed (*30*). Similar processes occurring beneath continents would provide the magma sources we hypothesize.

REFERENCES AND NOTES

1. G. King and M. Ellis, *Nature* **348**, 689 (1990).
2. I. A. Nairn and S. Beanland, *N. Z. J. Geol. Geophys.* **32**, 1 (1988).
3. C. J. N. Wilson and G. P. L. Walker, *Philos. Trans. R. Soc. London Ser. A* **314**, 199 (1985).
4. C. J. Ebinger, A. L. Deino, R. E. Drake, A. L. Tesha, *J. Geophys. Res.* **94**, 15785 (1989).
5. B. C. King, in *East African Magmatism*, I. Gass, Ed. (Oliver and Boyd, Edinburgh, 1970), pp. 263–282.
6. P. Mohr, *Tectonophysics* **143**, 169 (1987), and references therein; W. H. Morton, D. C. Rex, J. G. Mitchell, P. Mohr, *Nature* **280**, 284 (1979).
7. S. Horton and D. dePolo, personal communication.
8. D. P. Hill *et al.*, *Bull. Seismol. Soc. Am.* **80**, 325 (1990).
9. R. A. Bailey, *U.S. Geol. Surv. Open-File Rep. 77-468* (1977). Geothermal studies (including analysis of gravity and drill hole data) suggest that the original frontal fault system was farther to the east, placing Mammoth Mountain and associated volcanic centers unequivocally in the footwall [G. A. Suemnicht and R. J. Varga, *J. Geophys. Res.* **93**, 13191 (1988)].
10. B. R. Julian, *Nature* **303**, 323 (1983).
11. ———, *J. Geophys. Res.* **90**, 11155 (1985).
12. J. O. Langbein, D. P. Hill, T. N. Parker, S. K. Wilkinson, A. M. Pitt, *Eos* **43**, 1466 (1990).
13. W. Hildreth and G. A. Mahood, *Geol. Soc. Am. Bull.* **97**, 396 (1986).
14. P. W. Lipman, *Trans. R. Soc. Edinburgh Earth Sci.* **79**, 265 (1988), and references therein.
15. A. I. Kiselev, *Tectonophysics* **143**, 235 (1987) ———, H. A. Golovko, M. E. Medvedev, *ibid.* **45**, 49 (1978).
16. R. G. Bohannon, C. W. Naeser, D. L. Schmidt, R. A. Zimmerman, *J. Geophys. Res.* **94**, 1683 (1989).
17. R. E. Anderson, *Geol. Soc. Am. Abstr. Program* **20**, A115 (1988).
18. C. B. Hunt and D. R. Mabey, *U.S. Geol. Surv. Prof. Pap. 494-A* (1966).
19. G. W. Grindley, *Philos. Trans. R. Soc. London Ser. A* **274**, 165 (1973).
20. Carte Geologique de la France et de la Marge Continentale, Bureau de Recherche Geologique et Minière BP 6009, 45066, Orléans, Cedex.
21. The upper crust was modeled as an elastic plate with a density of 2700 kg m^{-3}, a thickness of 12 km, a crustal Young's modulus of 40 GPa, and an effective elastic thickness of ~3 km. The lower crust was assumed inviscid, with a density of 2900 kg m^{-3}. We further assumed 80% erosion and sedimentation at the earth's surface and an initial fault dip of 60°.
22. G. C. P. King, R. Stein, J. Rundle, *J. Geophys. Res.* **93**, 13307 (1988); R. Stein, G. C. P. King, J. Rundle, *ibid.*, p. 13319; R. G. Bilham and G. C. P. King, *ibid.* **94**, 10204 (1989).
23. D. A. Spence and D. L. Turcotte, *ibid.* **90**, 575 (1985); J. R. Lister and R. C. Kerr, *ibid.* **96**, 10049 (1991); A. M. Rubin and D. D. Pollard, *U.S. Geol. Surv. Prof. Pap. 1350* (1987), p. 1449.
24. J. M. Bartley, J. M. Fletcher, A. F. Glazner, *Tectonics* **9**, 521 (1990).
25. L. A. Wright *et al.*, *Geological Society of America Field Trip Guidebook* (Geological Society of America, Boulder, CO, in press).
26. W. Bosworth, *Geology* **15**, 397 (1987).
27. N. White, *ibid.* **17**, 111 (1989). White [*ibid.* **18**, 327 (1990)] also shows that simple-shear models of lithospheric extension make it extremely difficult to generate melt from the asthenosphere. W. R. Buck, F. Martinez, M. S. Steckler, S. R. Cochran, *Tectonics* **7**, 213 (1988); T. H. Dixon, E. R. Ivins, B. J. Franklin, *ibid.* **8**, 1193 (1989). In general, the simple-shear model advocated originally by B. Wernicke [*Can. J. Earth Sci.* **22**, 108 (1985)] has been superseded by models that involve more distributed shear within the lower crust [for example, G. S. Lister and G. A. Davis, *J. Struct. Geol.* **11**, 65 (1989)], to the extent that the Moho remains flat while the middle or lower crust is fluid [see (*1*) and B. Wernicke, in *Exposed Cross-Sections of the Continental Crust*, M. H. Salisbury and D. M. Fountain, Eds. (Kluwer Academic, Boston, 1990)].
28. C. J. Ebinger, T. D. Bechtel, D. W. Forsyth, C. O. Bowin, *J. Geophys. Res.* **94**, 2883 (1989). Estimates of effective elastic thickness determined from the geometry of footwall–hanging wall pairs along the western arm of the East African rift are of the order of 4 km [N. Kusznir and R. Westaway, *Eos* **71**, 1584 (1990)], which is close to that determined by King and Ellis (*1*) for the Basin and Range province, but in contrast to that of Ebinger's estimation.
29. M. Bursik and K. Sieh, *J. Geophys. Res.* **94**, 15587 (1989).
30. L. Fleitout and C. Moriceau, *Geophys. J. Int.*, in press.

31. This work was started while M. Ellis was at the Center for Neotectonic Studies, University of Nevada, Reno, and was supported then and while G. King was at the U.S. Geological Survey, Denver, CO, by the Nevada Nuclear Waste Projects Office. We are particularly grateful to R. E. Anderson, R. Thompson, R. Schweickert, B. Julian, R. Stein, and W. Mooney for insightful and constructive criticism and D. Matthews for editorial assistance.

3 June 1991; accepted 31 July 1991

Theoretical Fermi-Surface Properties and Superconducting Parameters for K_3C_{60}

STEVEN C. ERWIN AND WARREN E. PICKETT

Quantitative theories of superconductivity in alkali-doped C_{60} require an accurate and detailed description of the Fermi surface. First-principles calculations of Fermi-surface properties and electronic parameters for K_3C_{60}, the prototype fulleride-superconductor, are reported. The Fermi surface has two sheets; the first is free-electron-like, and the second is multiply-connected, forming two interlocked symmetry-equivalent pieces that never touch. The calculated (clean limit) London penetration depth is Λ = 1600 Å. Comparing the Fermi velocity with the experimental coherence length leads to a superconducting pairing strength $\lambda \sim 5$, indicating very strong coupling. Partial nesting in the second Fermi-surface sheet may favor coupling to short-wavelength $\langle q,0,0\rangle$ optic modes.

It is now well established that alkali-doping of C_{60} fullerenes leads to a class of solids, M_xC_{60} (M = alkali), that exhibit at least four crystalline phases, corresponding to $x = 0,3,4,6$. Theory and experiment show that both undoped C_{60} and fully-doped M_6C_{60} are molecular insulators, with predicted band gaps of 1.5 eV (*1*) and 0.5 eV (*2*), respectively. In striking contrast, M_3C_{60} forms a metallic superconducting phase, with transition temperatures (T_c) ranging from 18 K (M = potassium) (*3*) to 28 K (M = rubidium) (*4*), and even higher for Cs-Rb alloys (*5*). Recent theoretical attention has focused on electron-phonon coupling as a possible mechanism for superconductivity (*6, 7*). It is well known that the coupling strength and critical temperature are strongly influenced by zone-averaged electronic properties, such as the Fermi-level density of states. However, the shape of the Fermi surface may also play a significant role, by giving rise to wavevector anisotropies in the quasiparticle-pairing strength, as for the La_2CuO_4-based superconductors (*8*). Here we report the results of our first-principles calculations of the Fermi surface and of electron dynamics in K_3C_{60}, and of the coupling strength λ implied by our results and experimental data.

Rietveld analysis of powder x-ray diffraction data for K_3C_{60} reveals a simple face-centered cubic (fcc) Bravais lattice, with K atoms located at the tetrahedral and octahedral interstitial sites (*9*). The best fit was achieved with C_{60} molecules placed randomly in two orientations, each populated

S. C. Erwin, Department of Physics, University of Pennsylvania, Philadelphia, PA 19104–6272.
W. E. Pickett, Complex Systems Theory Branch, Code 4692, Naval Research Laboratory, Washington, DC 20375–5000.